CHAPTER IV

Double layer and sandwiched magneto-dielectric absorbers using strontium ferrite-LLDPE

Content:

4.1 Introduction

Bandwidth of an absorber can be enhanced by augmenting number of layers without appreciable increase on the total thickness of the absorbing structure [1-6]. Multilayering reduces reflection, by progressively profiling the impedance from that of free space to a lossy medium [7-9]. Controlling the magnetic and dielectric loading of individual layers can lead to enhanced absorption bandwidth. Double layer microwave absorber reported in shows improvement in matching condition and hence in absorption bandwidth.

The first multilayer absorber reported was the Jaumann absorber, where alternate resistive sheets were spaced a quarter wavelength apart by uniform air gaps increasing the bandwidth over the Salisbury single resistive sheet [10, 11]. The bandwidth could be further enhanced by modifying the magnetic and dielectric properties of the layers so as to customize the effective admittance [12].

Two different multilayer structures are designed and studied - (i) a conventional double-layer microwave absorber and ii) a triple layer structure where a dielectric layer is sandwiched between two magneto-dielectric layers. The -10 dB absorption bandwidth studies carried out on single layer absorbers in the previous chapters of the three compositions are given in table 3.6, section 3.4.2. 60 wt. % of $SrFe_{12}O_{19}$-LLDPE and $SrCo_{0.8}Fe_{11.2}O_{19}$-LLDPE composites show better absorption than 60 wt. % $SrAl_2Fe_{10}O_{19}$-LLDPE and are used as the two magneto-dielectric layers. Transmission line model (TL model) is used to estimate the absorption properties of the structures for different thicknesses and to identify the combination of thickness which is likely to result in the maximum absorption. Based on these estimations, the multilayer structures are fabricated with different thickness combinations and their absorption performance evaluated experimentally.

4.2 Double layer absorber

4.2.1 Design of a double layer absorber

The schematic diagram of a conductor backed two layer absorber is shown in figure 4.1.

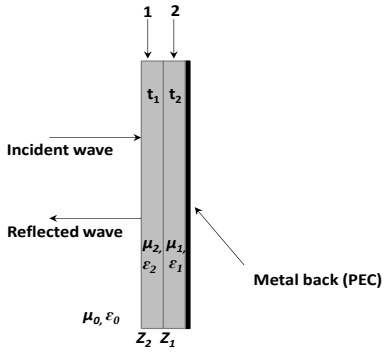

Figure 4.1: Schematic of double layer microwave absorber

Reflection loss (*RL*) estimated using TLM is given by

$$RL\ (dB) = 20 \log \left| \frac{Z_{in} - Z_0}{Z_{in} + Z_0} \right| \tag{4.1}$$

where, Z_{in} is the input impedance of the transmission line given by

$$Z_{in} = \eta_i \frac{Z_{i-1} + \eta_i \tanh \gamma_i t_i}{\eta_i + Z_{i-1} \tanh \gamma_i t_i} \tag{4.2}$$

Here, $\eta_2 = \eta_0 \sqrt{\mu_{r_i} / \varepsilon_{r_i}}$ is the intrinsic impedance of the 2nd layer, $\gamma_i = j \frac{2\pi f}{c} \sqrt{\varepsilon_{r_i} \mu_{r_i}}$ being the propagation constant, $\varepsilon_r\ (\varepsilon_r = \varepsilon_r' - j\varepsilon_r'')$, $\mu_r\ (\mu_r = \mu_r' - j\mu_r'')$ are the complex permittivity and complex permeability respectively, t_1 and t_2 the thickness of the absorbing layers 1 & 2 respectively and Z_0 the characteristic impedance of free space. The input impedance at the air absorber interface, Z_2, and the reflection loss of a two layer absorber is given by [13, 14]

$$Z_2 = \eta_2 \frac{\eta_1 \tan h\, \gamma_1 t_1 + \eta_2 \tan h\, \gamma_2 t_2}{\eta_2 + \eta_1 \tan h\, (\gamma_1 t_1)\ \tan h\, (\gamma_2 t_2)} \tag{4.3}$$

$$RL = \left| \frac{\sqrt{\mu_{r_2}/\varepsilon_{r_2}} \left[\frac{\sqrt{\mu_{r_1}/\varepsilon_{r_1}} \tan h \left(j\frac{2\pi f}{c} \right) \sqrt{\mu_{r_1}\varepsilon_{r_1}} t_1 + \sqrt{\mu_{r_2}/\varepsilon_{r_2}} \tan h \left(j\frac{2\pi f}{c} \right) \sqrt{\mu_{r_2}\varepsilon_{r_2}} t_2}{\sqrt{\mu_{r_2}/\varepsilon_{r_2}} + \sqrt{\mu_{r_1}/\varepsilon_{r_1}} \tan h \left(j\left(\frac{2\pi f}{c}\right) \sqrt{\mu_{r_1}\varepsilon_{r_1}} t_1 \right) \tan h \left(j\left(\frac{2\pi f}{c}\right) \sqrt{\mu_{r_2}\varepsilon_{r_2}} t_2 \right)} \right] - 1}{\sqrt{\mu_{r_2}/\varepsilon_{r_2}} \left[\frac{\sqrt{\mu_{r_1}/\varepsilon_{r_1}} \tan h \left(j\frac{2\pi f}{c} \right) \sqrt{\mu_{r_1}\varepsilon_{r_1}} t_1 + \sqrt{\mu_{r_2}/\varepsilon_{r_2}} \tan h \left(j\frac{2\pi f}{c} \right) \sqrt{\mu_{r_2}\varepsilon_{r_2}} t_2}{\sqrt{\mu_{r_2}/\varepsilon_{r_2}} + \sqrt{\mu_{r_1}/\varepsilon_{r_1}} \tan h \left(j\left(\frac{2\pi f}{c}\right) \sqrt{\mu_{r_1}\varepsilon_{r_1}} t_1 \right) \tan h \left(j\left(\frac{2\pi f}{c}\right) \sqrt{\mu_{r_2}\varepsilon_{r_2}} t_2 \right)} \right] + 1} \right| \tag{4.4}$$

The reflection loss is first computed using the equation (4.4) and thereafter, measured to compare with the computed values.

4.2.2 Absorption studies of the double layer structure

The double layer structure consists of the ferrite compositions which are given in the table 4.1.

Table 4.1: Selection of ferrite-LLDPE nanocomposites for double layer design combinations

Ferrite composition	Designation	Resonant frequency f_r (GHz)	Max. absorption at f_r (dB)	-10 dB bandwidth (GHz)
60 wt.%, $SrFe_{12}O_{19}$-LLDPE	**A**	10.5	-22.0	3.36 (8.53-11.89 GHz)
60 wt.%, $SrCo_{0.8}Fe_{11.2}O_{19}$-LLDPE	**B**	9.3	-23.2	3.56 (8.84-12.4 GHz)

Theoretical computation of reflection loss of the double layer structure is studied with optimized thickness. Based on the theoretical results, a double layer metal backed absorber is fabricated and tested for microwave absorption over the X-band.

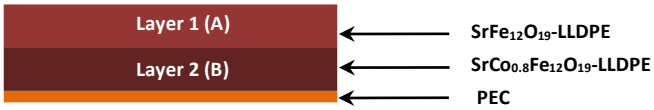

Figure 4.2: Schematic of conductor backed double layer absorber structure

Computed microwave absorption

The microwave absorption of the double layer absorbing structure is computed using TL Model.

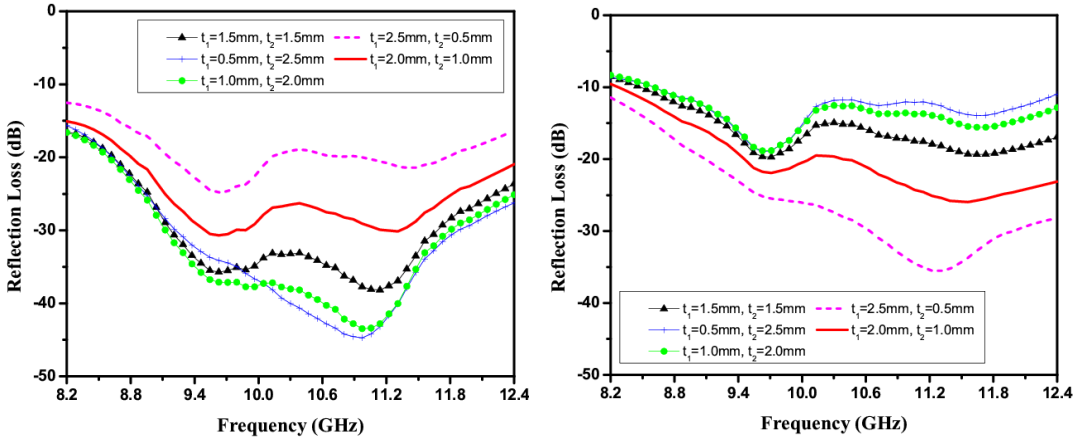

Figure 4.3: Plots of RL_c of conductor backed double layer absorber structure **(a)** AB **(b)** BA

Double layer combination of AB layers having air-absorber interfacing layer as B, i.e., layer 1 as $SrFe_{12}O_{19}$-LLDPE composite and layer 2 as $SrCo_{0.8}Fe_{11.2}O_{19}$-LLDPE composite and another combination as BA where A is the air-absorber interface layer.

Keeping the total thickness of the absorber as:

$$t = t_1 + t_2 = 3\ mm \tag{4.5}$$

optimization of different compositions and the thicknesses of composite layers have been carried out to obtain the minimum value of reflection loss (RL_c) and absorption over the X-band. The thickness of cobalt and aluminium substituted strontium ferrite composite samples were optimized for broad -10 dB bandwidth using transmission line model (TL model) for different thickness (Table 3.5 and Table 3.6, chapter III). It was found that in most of the results 3 mm sample thickness gave the best results also satisfying the condition of destructive interference at a particular frequency (t= λ/4). However, for some of the samples with thickness > 3 mm also showed similar absorption results along with the 3 mm samples. For better comparison among all the fabricated prototypes both single and multilayer, the total thickness of multilayered structure was kept same. The individual thickness of layers t_1 and t_2 is varied for different combinations for a step size of 0.5 mm confirming to equation (4.5). The minimum thickness of the individual layer is kept at 0.5 mm considering the fabrication limits of the absorber layer. Using equation (4.2) and the measured values of complex permittivity and permeability, RL_c of the conductor backed double layer absorber is computed. Figure 4.3 shows the plots of RL_c with different design combinations and layer composition which is detailed in table 4.2.

Table 4.2: RL_c with -10 dB calculated absorption bandwidth (BW_c) values

Absorber structures	**Thickness (t) of individual layers (mm)**		**Maximum RL and corresponding frequency**		**Bandwidth (GHz)**	
	t_1	t_2	RL_c (dB)	f_r (GHz)	-10 dB BW_c	-20 dB BW_c
AB	0.5	2.5	-42.98	11.14	4.20	3.78
	1.0	2.0	-26.59	9.71	4.20	2.43
	1.5	1.5	-46.05	11.14	4.20	3.78
	2.0	1.0	-32.55	11.14	4.20	3.53
	2.5	0.5	-48.04	11.14	4.20	3.78
BA	0.5	2.5	-21.73	9.71	3.86	-
	1.0	2.0	-21.18	9.71	3.78	-
	1.5	1.5	-21.37	9.71	3.78	-
	2.0	1.0	-26.17	11.39	4.12	2.85
	2.5	0.5	-36.10	11.22	4.20	3.36

From the optimization carried out for the absorber structures, the combinations with the highest bandwidths are selected for fabrication and testing which are highlighted in table 4.2.

The prepared hexagonal ferrite powder of composition $SrFe_{12}O_{19}$ and of composition $SrCo_{0.8}Fe_{11.2}O_{19}$, are mechanically blended with LLDPE powder to obtain a homogeneous mixture with weight percentage of 60. The mixture of $SrFe_{12}O_{19}$-LLDPE is then put in a three-piece die-mould which is initially heated up to 90˚C. A pressure up to 36.0 MPa is applied and is isothermally heated upto 110˚C and kept for a duration of 45 minutes. Thereafter, the mixture of $SrCo_{0.8}Fe_{11.2}O_{19}$-LLDPE is put on top of the first layer in the die-mould and is cured for the same pressure at 110˚C for 45 minutes. The die-mould is cooled at room temperature.

Measured microwave absorption

The fabricated sample is placed inside an X-band sample holder (WR-90 X11644A) terminated by a metal plate (short). The measured reflection loss (RL_m) values of the fabricated samples are plotted in figure 4.4.

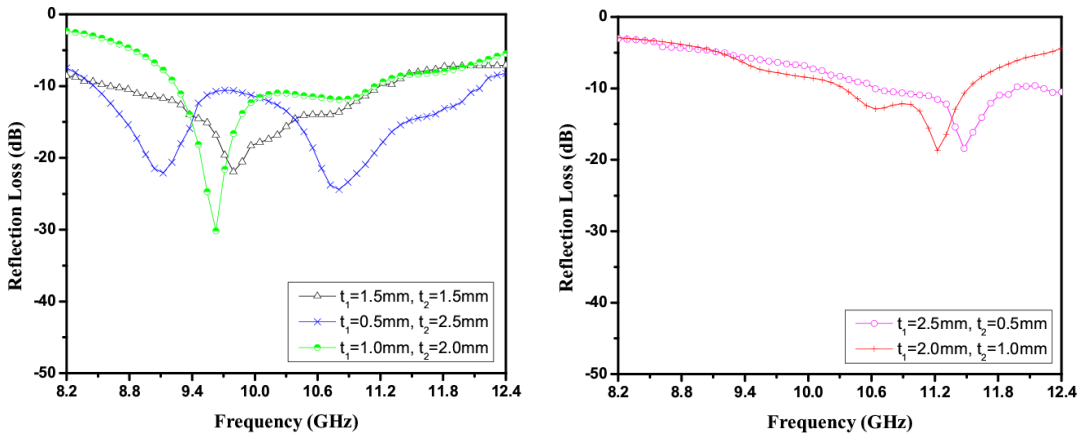

Figure 4.4: Measured reflection loss (RL_m) of fabricated conductor backed double layer absorber structure **(a)** AB **(b)** BA (figure 4.2)

From the graphs, it is observed that for the combination of $t_1 = 0.5$ and $t_2 = 2.5$, the reflection loss is maximum for the layer combination of AB which is also seen from the theoretical computations.

Table 4.3: Measured reflection loss (RL_m) with absorption bandwidth (BW_m) values

Absorber structures	t_1	t_2	RL_m (dB)	f_{r1} (GHz)	f_{r2} (GHz)	-10 dB BW_m (GHz)
AB	0.5	2.5	-21.92	9.79	---	2.69
	1.5	1.5	-30.18	9.63	---	2.02
	2.5	0.5	-24.40	9.10	10.80	3.69
BA	2.0	1.0	-18.69	11.22	---	1.34
	2.5	0.5	-18.61	11.47	---	1.93

A maximum reflection loss of -24.4 dB and -10 dB absorption bandwidth of 3.69 GHz (8.45-12.14 GHz) is obtained (Figure 4.4 (a)). It is seen that for the combination t_1=2.5 mm and t_2 = 0.5 mm, double absorption peaks are observed. Since the permittivity of the second layer is greater than the first layer over the X-band (Figure 2.13 and 3.12), the incident EM wave when passing from layer 1 to layer 2 experiences some impedance discontinuity because of difference in the permittivity values. Hence, a part of the *em* wave will get reflected back from the layer 1and 2 interface. From the studies conducted on the reflection loss of 60 wt. % $SrFe_{12}O_{19}$-LLDPE (Figure 2.18 (b)), it is seen that the reflected wave emerging from the interface nearly satisfies λ/4 condition for destructive interference, for a thickness of 2.5 mm giving calculated reflection loss of -40.4 dB at resonant frequency (f_r) of 12.1 GHz. The reflected wave emerging from the layer 1 and 2 interface and that from the overall double layer structure couples together to give double absorption peak and broad -10 dB bandwidth. No significant increase in the reflection loss values and in absorption bandwidth is observed for the layer combination of BA (Figure 4.4 (b)). The frequency of maximum peak of measured and calculated minimum reflection loss shows close proximity. However, the experimental reflection loss values are lower than the theoretical reflection loss value for all the combinations as seen from table 4.3. Table 4.4 presents absorption performance of some of the reported works on double layer absorbers in X-band, along with the present work.

Table 4.4: Comparison of microwave absorbing properties of reported double-layer absorbers

Material composition	*t* (mm)	Max RL (dB)		-10 dB bandwidth (GHz)	
		Theor.	Exp.	Theor.	Exp.
$BaCo_{0.8}Ti_{0.8}Mn_{0.1}Fe_{10.27}O_{19}$, $(Ba(MnTi)_{1.6}Fe_{8.8}O_{19}$ in epoxy resin [14]	1.0	-	-13.00	-	1.50
$BaCo_{0.4}Zn_{1.6}Fe_{16}O_{27}$ ferrite and carbonyl iron powder in epoxy resin [15]	2.3	-55.40	-	5.2	-
$BaZn_{0.6}Zr_{0.3}Ti_{0.3}Fe_{10.8}O_{19}$, $BaZn_{0.6}Zr_{0.3}Ce_{0.3}Fe_{10.8}O_{19}$, $BaZn_{0.6}Zr_{0.3}Sn_{0.3}Fe_{10.8}O_{19}$ in rubber and epoxy resin [16]	5.0	-	-10.80	-	1.2
Present work	**3.0**	-48.04	**-24.40**	4.2	**3.69**

4.3 Sandwich layer absorber

A three layer structure comprising of a dielectric layer sandwiched between two magneto-dielectric layers. The schematic of the proposed absorber structure is given in figure 4.5 (a & b). One of the two magneto-dielectric layers is perfect electric conductor (PEC) backed while the other acts as a matching mechanism at the air-absorber interface. The material property of the sandwitched layer can effectively control the impedance of the air absorber interface, attenuation of the EM wave and thickness of the absorber. With a proper choice of material for the outer layers and the sandwitched layer, a wide absorption bandwidth can be achieved. EM wave incident at the air-Layer 3 interface penetrates into Layer 3 (A) and attenuates through the three layers reaching the PEC, getting reflected and again attenuates through the layers reaching the air-Layer 3 interface. This process repeats resulting in multiple reflections leading to enhanced absorption. Use of magneto-dielectric material as Layer 1 (B) with both dielectric and magnetic loss effectively attenuates the wave within the structure [17, 18]. A dielectric layer (Layer 2) between the two magneto-dielectric layers improves matching. In addition, the complex permittivity of the dielectric layer can be adjusted by adding expanded graphite (EG) [1]. A high value dielectric layer reduces overall thickness of the absorber and increases attenuation.

Here, the use of the same matrix (LLDPE) in all the three layers aids in the fabrication process due to easier adhesion between layers.

Transmission line model is used to estimate the absorption properties of the three layer structure for different thicknesses and to identify the combination of thickness. Based on these estimations, the multilayer structures are fabricated with different thickness combinations and their absorption performance evaluated experimentally.

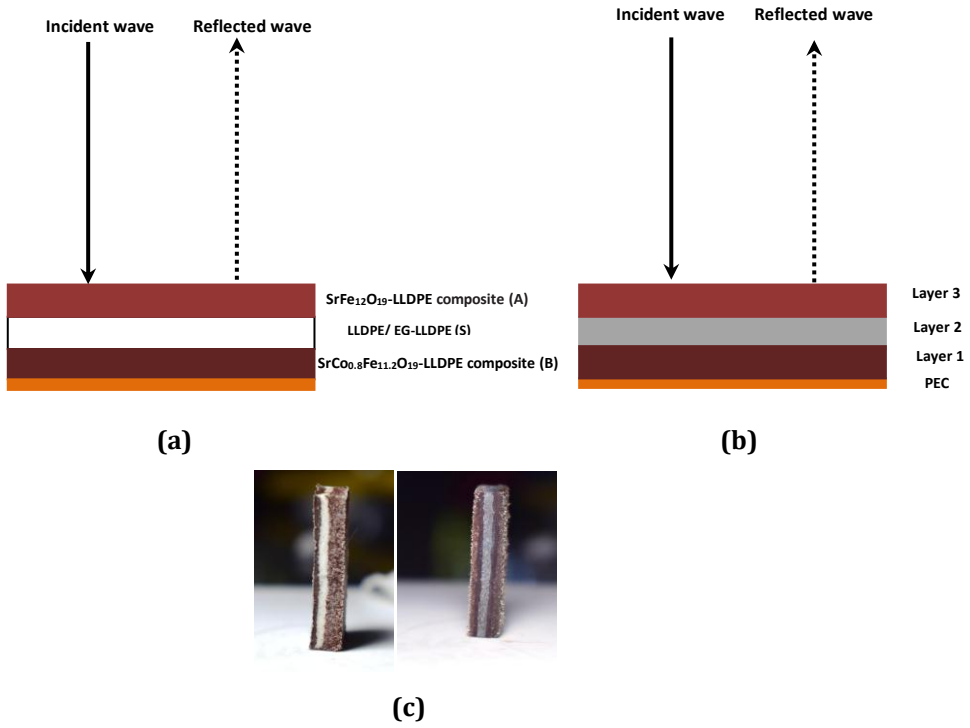

Figure 4.5: Triple layer sandwiched absorber:
(a) LLDPE as Layer 2 **(b)** EG-LLDPE as Layer 2 **(c)** Fabricated composites

4.3.1 Design of a sandwiched layer absorber using transmission line model

The sandwiched microwave absorber is designed using the principles of multilayer absorber. Reflection loss (*RL*) is estimated using TLM;

$$RL(dB) = 20\log\left|\frac{Z_{in}-Z_0}{Z_{in}+Z_0}\right| \tag{4.6}$$

where, Z_{in} is the input impedance of the transmission line given by

$$Z_{in} = \eta_i \frac{Z_{i-1}+\eta_i \tanh \gamma_i t_i}{\eta_i + Z_{i-1}\tanh \gamma_i t_i} \tag{4.7}$$

Here, $\eta_i = \eta_0\sqrt{\mu_{r_i}/\varepsilon_{r_i}}$ is the intrinsic impedance of the ith layer, $\gamma_i = j\frac{2\pi f}{c}\sqrt{\varepsilon_{r_i}\mu_{r_i}}$ being the propagation constant, f the microwave frequency, ε_r ($\varepsilon_r = \varepsilon_r' - j\varepsilon_r''$),

$\mu_r (\mu_r = \mu_r' - j\mu_r'')$ are the complex permittivity and complex permeability respectively, t_i the thickness of the ith (i = 1, 2, 3…) constituent layer and Z_0 the characteristic impedance of free space. For a three layer absorber [19, 20], equivalent input impedance and the reflection loss of the absorber is given by;

$$Z_{in} = Z_3 = \eta_3 \left[\frac{\eta_2 \frac{\eta_1 \tanh\gamma_1 t_1 + \eta_1 \tanh\gamma_2 t_2}{\eta_3 + \eta_1 \tanh\gamma_1 t_1 \tanh\gamma_2 t_2} + \eta_3 \tanh\gamma_3 t_3}{\eta_3 + \eta_2 \frac{\eta_1 \tanh\gamma_1 t_1 + \eta_1 \tanh\gamma_2 t_2}{\eta_2 + \eta_1 \tanh\gamma_1 t_1 \tanh\gamma_2 t_2} \tanh\gamma_3 t_3} \right] \tag{4.8}$$

$$RL_c = 20log \left| \frac{\eta_3 \frac{\eta_2 \frac{\eta_1 tanh\gamma_1 t_1 + \eta_2 tanh\gamma_2 t_2}{\eta_3 + \eta_1 tanh(\gamma_1 t_1) tanh(\gamma_2 t_2)} + \eta_3 tanh\gamma_3 t_3}{\eta_2 + \eta_1 tanh(\gamma_1 t_1) tanh(\gamma_2 t_2)} - \eta_0}{\eta_3 + \eta_2 \frac{\eta_1 tanh\gamma_1 t_1 + \eta_2 tanh\gamma_2 t_2}{\eta_2 + \eta_1 tanh(\gamma_1 t_1) tanh(\gamma_2 t_2)} tanh\gamma_3 t_3} \right| \tag{4.9}$$

$$\eta_3 \frac{\eta_2 \frac{\eta_1 tanh\gamma_1 t_1 + \eta_2 tanh\gamma_2 t_2}{\eta_3 + \eta_1 tanh(\gamma_1 t_1) tanh(\gamma_2 t_2)} + \eta_3 tanh\gamma_3 t_3}{\eta_2 + \eta_1 tanh(\gamma_1 t_1) tanh(\gamma_2 t_2)} + \eta_0$$

where, $\eta_1 = \eta_0\sqrt{\mu_{r1} / \varepsilon_{r1}}$, $\eta_2 = \eta_0\sqrt{\mu_{r2} / \varepsilon_{r2}}$, $\eta_3 = \eta_0\sqrt{\mu_{r3} / \varepsilon_{r3}}$, $\gamma_1 = 2\pi f c)\sqrt{\mu_{r1}\varepsilon_{r1}}$, $\gamma_2 = j(2\pi f / c)\sqrt{\mu_{r2}\varepsilon_{r2}}$, $\gamma_3 = j(2\pi f/c)\sqrt{\mu_{r3}\varepsilon_{r3}}$.

The layer 1 with thickness t_1 and material parameter $\varepsilon_{r1}, \mu_{r1}, \eta_1, \gamma_1$ is the interface layer, layer 2 with thickness t_2 and material parameter $\varepsilon_{r2}, \mu_{r2}, \eta_2, \gamma_2$ is the sandwiched layer and layer 3 with thickness t_3 and material parameter $\varepsilon_{r3}, \mu_{r3}, \eta_3, \gamma_3$ is in vicinity to the metal plate. Thus, material properties and the thicknesses (t_1, t_2 and t_3) of the layers are prime factors which influence the absorption.

The complex permittivity and complex permeability values of EG-LLDPE composites and LLDPE are measured and is given in table 4.5.

Table 4.5: Complex permittivity and Complex permeability of the composites

Material parameters / **Layer 2 (S)**	**Weight fraction**	ε_r'	ε_r''	μ_r'	μ_r''
LLDPE	0 wt.%	2.01	0.02	0.99	0.0001
EG-LLDPE composite	5 wt. %	2.80	0.40	0.99	0.0001
	7 wt. %	4.80	0.90	0.99	0.0001
	8 wt. %	5.30	1.30	0.99	0.0001

The studies of EG doped LLDPE composite is confined to 5, 7 & 8 wt. % as in a similar study carried out based on EG-NPR composites, a significant absorption bandwidth reduction is observed as EG % is increased beyond 10 wt. % [1].

4.3.2 Absorption studies of the sandwiched layer structure

Theoretical computation of reflection loss of the sandwiched layer structure is studied with optimized thickness. Based on the theoretical results, a sandwiched metal backed absorber is fabricated and tested for microwave absorption over the X-band.

Computed microwave absorption using TLM

The thicknesses of the three layers are optimized to obtain the best absorption performance with the overall thickness of the sandwiched absorber maintained at 3 mm. Good absorption performance has been reported for a thickness of 3 mm in the case of single layer absorber (in the earlier chapters). The current work concentrates on further enhancement of absorption and bandwidth without increasing the absorber thickness.

In the first structure (figure 4.5 a), Layer 1 (designated as B) is taken as $SrFe_{12}O_{19}$-LLDPE composite, Layer 2 (designated as S) as LLDPE layer and $SrCo_{0.8}Fe_{11.2}O_{19}$-LLDPE composite as Layer 3 (designated as A) resulting in a structure that can be described as an ASB structure. Subsequently (figure 4.5 b), the layer 2 is replaced by 5 wt. %, 7 wt. % and 8 wt. % of EG-LLDPE composite, the complete structure is designated as AS_5B, AS_7B and AS_8B, respectively.

The thickness of each of the three layers A, S and B, are varied in the range of 0.5 mm to 2.0 mm in steps of 0.5 mm and reflection loss is calculated for each of the structures (figure 4.6 to 4.9). Here, only those results are included which show -10 dB absorption bandwidth for all the structures.

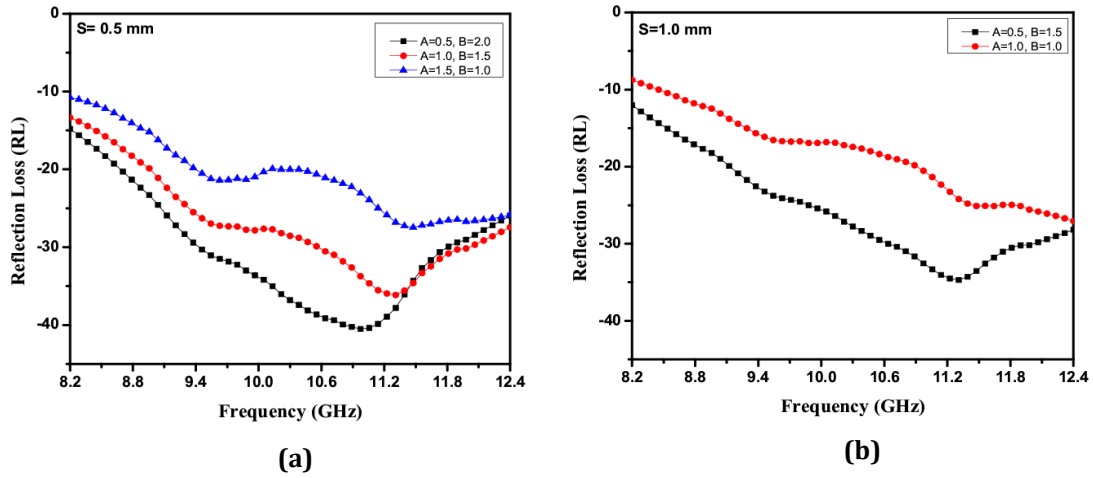

Figure 4.6: Frequency vs. Computed reflection loss (RL_c) plot of conductor backed triple layer absorber (ASB) with Layer 2 as LLDPE with t **(a)** 0.5 mm **(b)** 1.0 mm

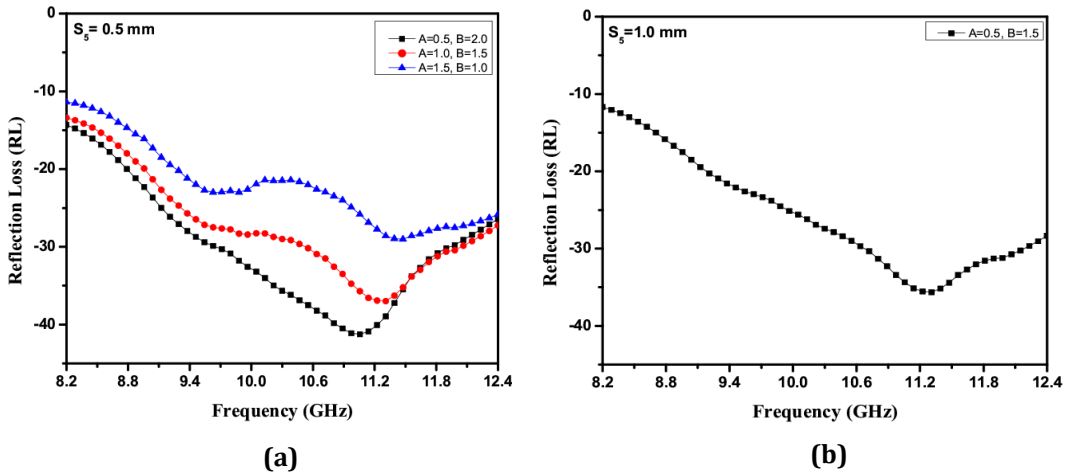

Figure 4.7: Frequency vs. Computed reflection loss (RL_c) plot of conductor backed triple layer absorber (AS_5B) with Layer 2 as 5 wt. % of EG-LLDPE with t **(a)** 0.5 mm **(b)** 1.0 mm

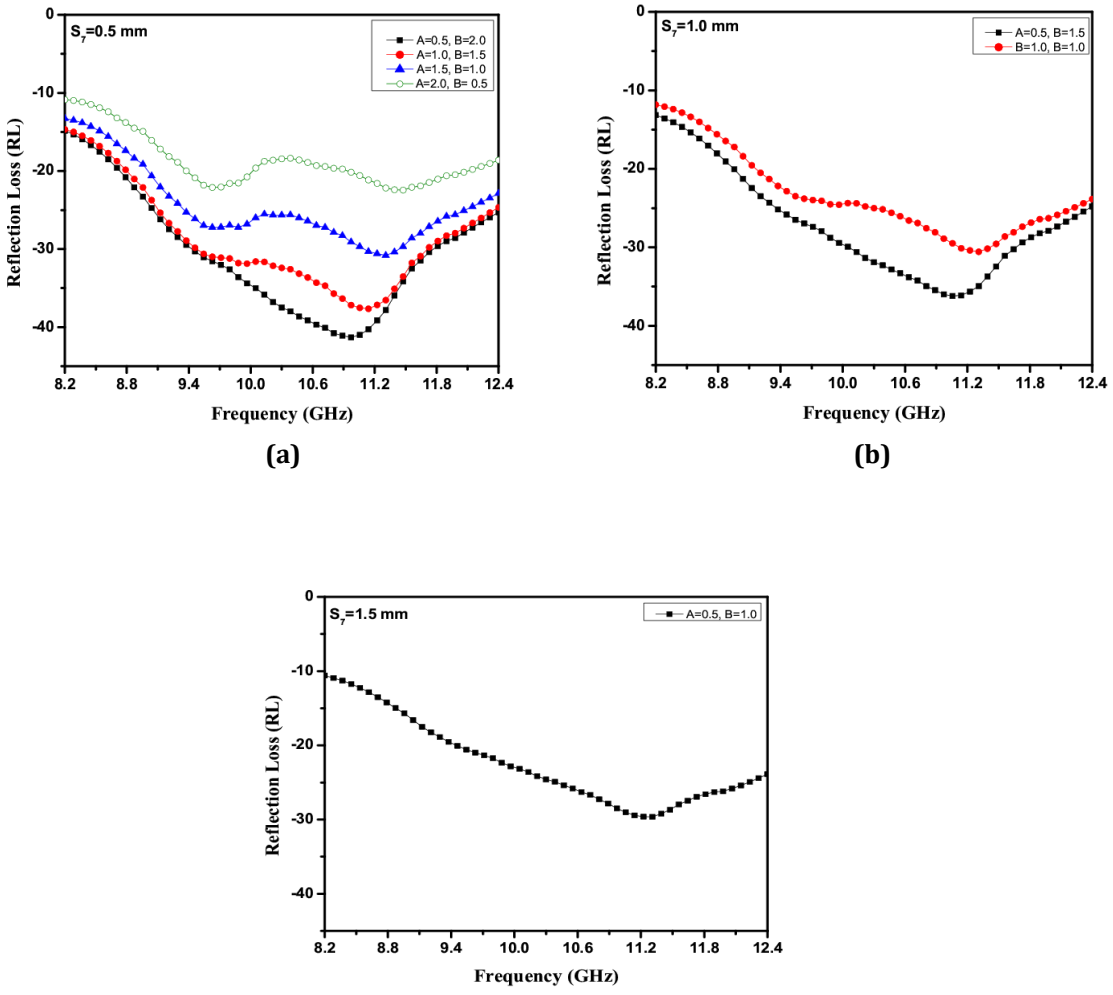

Figure 4.8: Frequency vs. Computed reflection loss (RL_c) plot of conductor backed triple layer (AS_7B) with Layer 2 as 7 wt. % of EG-LLDPE with t **(a)** 0.5 mm **(b)** 1.0 mm **(c)** 1.5 mm

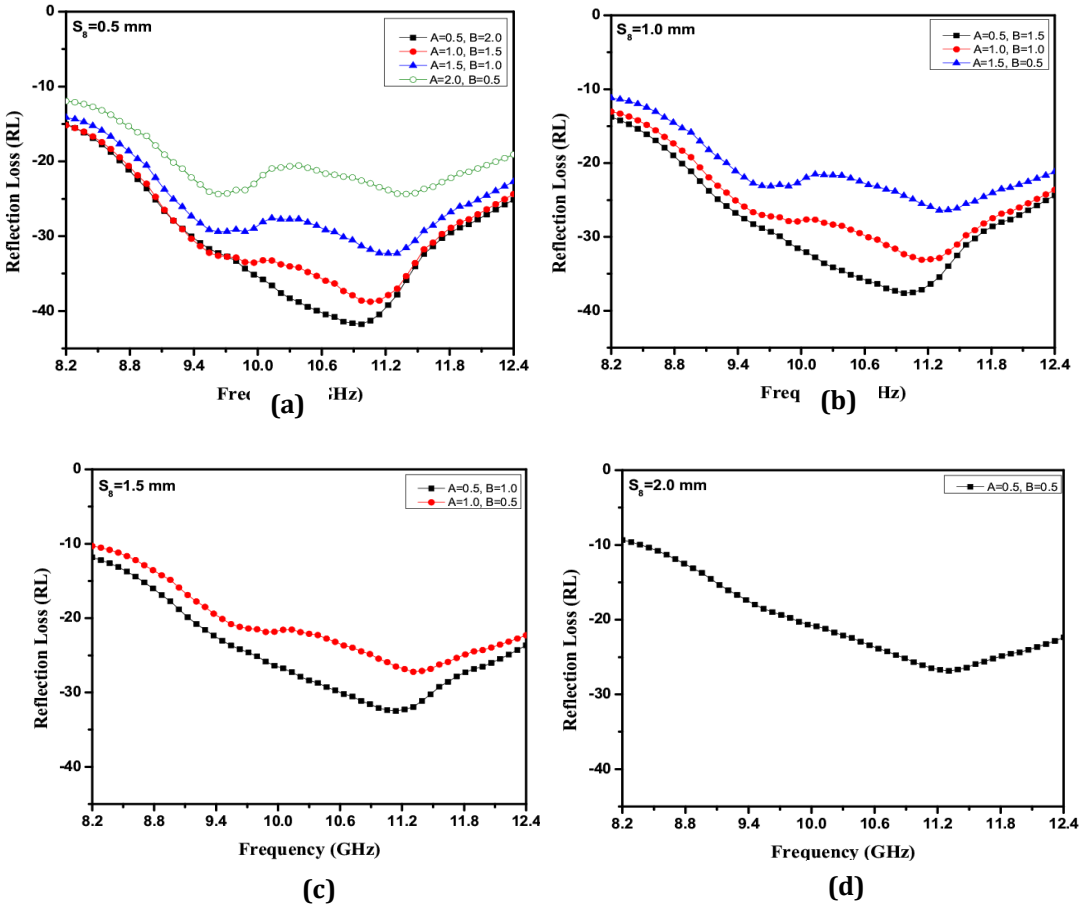

Figure 4.9: Frequency vs. Computed reflection loss (RL_c) plot of conductor backed triple layer absorber (AS_8B) with Layer 2 as 8 wt. % of EG-LLDPE with t **(a)** 0.5 mm **(b)** 1.0 mm **(c)** 1.5 mm **(d)** 2.0 mm

From table 4.6, it can be seen that samples for all the four structures (highlighted in the table) with A = 0.5, S = 0.5, B = 2.0 mm, show best performance and hence samples are fabricated with these structural dimensions. The sandwiched structure is prepared by laying one layer over the other. Interlayer adhesion is achieved by lightly pressing and curing at a temperature above the glass transition temperature of LLDPE. This process ensures minimal cross-layer contamination.

Nanosized $SrFe_{12}O_{19}$, and nanosized $SrCo_{0.8}Fe_{11.2}O_{19}$ powder in 60 wt. % is mechanically blended with sieved LLDPE powder, to obtain material composites for A and B layers respectively. In structure 2, for S layer, EG is blended with LLDPE powder. The bottom of a rectangular mould of standard X-band waveguide cross section dimension (10.38 mm x 22.94 mm) is first layered with $SrFe_{12}O_{19}$-LLDPE composite Layer A upto the required thickness and cured at

90˚C with a constant pressure of 36.5 MPa for 40 minutes. LLDPE or EG-LLDPE composite which is then used to obtain the required thickness for layer S on top of the A layer and again cured at the same temperature, pressure and duration as is done for A layer. Finally the last layer, $SrCo_{0.8}Fe_{11.2}O_{19}$-LLDPE composite is added as B layer and the curing process is carried out at a temperature of 110˚C with the same pressure and duration.

Table 4.6: Computed Reflection loss (RL_c) and Banwidth (BW_c) using TL model

Absorber composition (figure 4.5)	**Thickness (t) of individual layers (mm)**			**Maximum RL and corresponding frequency**		**Bandwidth (GHz)**	
	A	S	B	RL_c (dB)	f_r (GHz)	-10 dB BW_c	-20 dB BW_c
ASB	0.5	0.5	2.0	-42.21	11.14	4.2	3.60
	1.0	0.5	1.5	-37.83	11.14	4.2	3.45
	1.5	0.5	1.0	-28.67	11.47	4.2	3.03
	0.5	1.0	1.5	-35.23	11.14	4.2	3.19
	1.0	1.0	1.0	-26.25	12.23	4.2	1.43
AS_5B	0.5	0.5	2.0	-43.36	11.14	4.2	3.53
	1.0	0.5	1.5	-39.11	11.14	4.2	3.44
	1.5	0.5	1.0	-30.36	11.47	4.2	3.11
	0.5	1.0	1.5	-36.46	11.14	4.2	3.11
AS_7B	0.5	0.5	2.0	-42.75	11.14	4.2	3.61
	1.0	0.5	1.5	-41.21	11.14	4.2	3.53
	1.5	0.5	1.0	-31.21	11.47	4.2	3.36
	2.0	0.5	0.5	-23.62	11.47	4.2	0.59, 0.59
	0.5	1.0	1.5	-38.01	11.14	4.2	3.44
	1.0	1.0	1.0	-32.04	11.14	4.2	3.19
	0.5	1.5	1.0	-30.56	11.14	4.2	3.02
AS_8B	0.5	0.5	2.0	-42.94	11.14	4.2	3.63
	1.0	0.5	1.5	-42.54	11.14	4.2	3.61
	1.5	0.5	1.0	-35.20	11.14	4.2	3.44
	2.0	0.5	0.5	-25.54	11.47	4.2	1.76, 0.92
	0.5	1.0	1.5	-39.20	11.14	4.2	3.44
	1.0	1.0	1.0	-35.62	11.14	4.2	3.36
	1.5	1.0	0.5	-27.47	11.47	4.2	3.11
	0.5	1.5	1.0	-33.94	11.14	4.2	3.19
	1.0	1.5	0.5	-28.01	11.14	4.2	3.02
	0.5	2.0	0.5	-27.38	11.14	4.2	2.52

Measured microwave absorption

The prepared sample is removed from the die-mould and placed next to a terminating metal back of length 97.8 cm and thickness 0.03 mm. The RL_m values and the percentage absorption of the fabricated samples as a function of frequency

are plotted in figure 4.10 (a-d). The percentage absorption is calculated using the following formula, $Absorption\ (\%) = 100\left[1 - 10^{\frac{RL\ (dB)}{10}}\right]$.

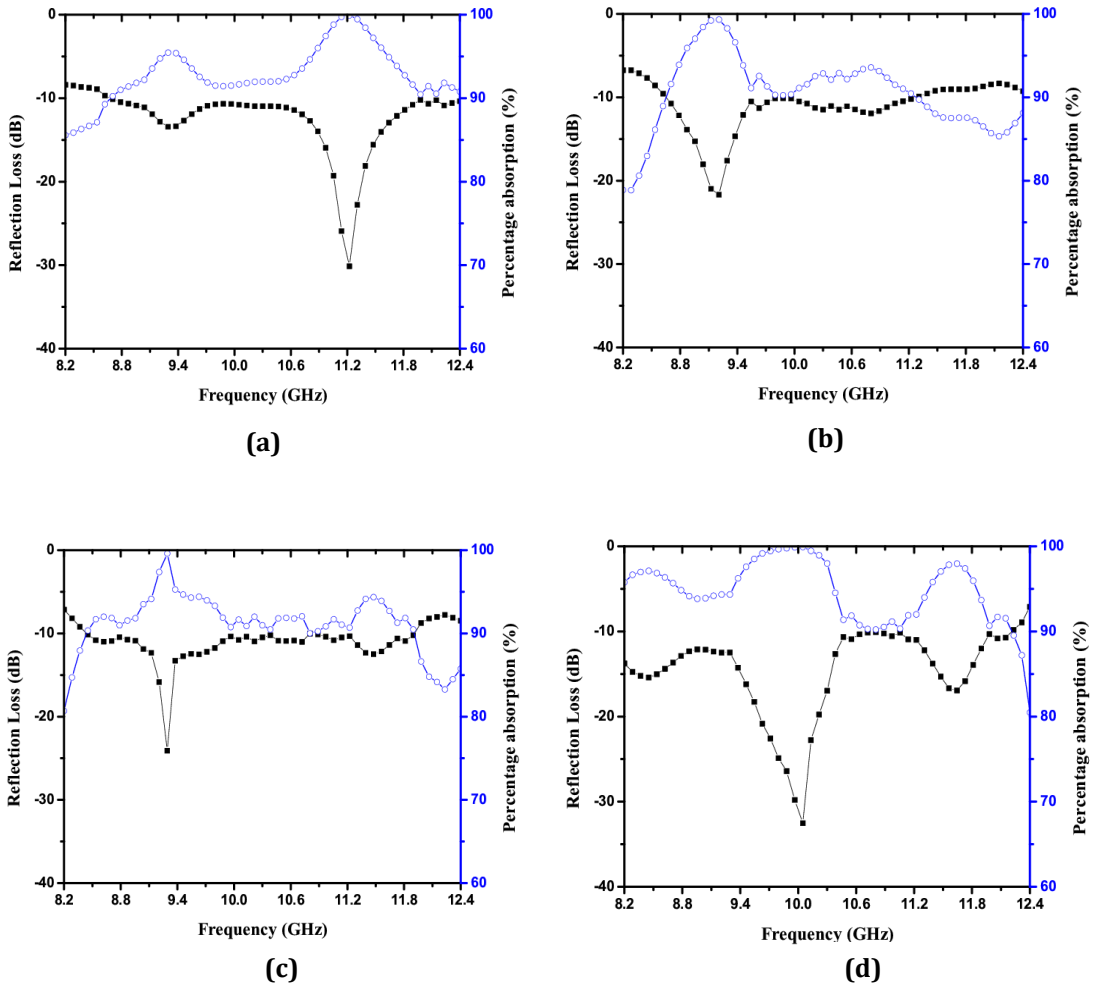

Figure 4.10: Frequency vs. Measured reflection loss (RL_m) plot & percentage absorption plots of fabricated triple layer sandwich absorber **(a)** ASB **(b)** AS_5B **(c)** AS_7B **(d)** AS_8B

The measured results demonstrate the role of impedance matching on the overall absorption performance of the developed absorbers. In figure 4.9 (a-d), it is seen that AS_8B structure enhances absorption among all the four structures. This may be due to attenuation of the wave which can be attributed to better impedance match at the air-absorber interface and multiple reflections within the structure having relatively similar material parameters as compared to the other three. The measured reflection loss plots also exhibit prominent absorption peaks, indicating maximum microwave absorption occurring at the matching thickness, *t*, of the multilayer structure. As the EG percentage is increased from zero (i.e., only

LLDPE) to 8 %, initially the -10 dB absorption bandwidth decreases when EG increases from 0 to 5 % and subsequently increases with increasing EG % reaching a maximum for 8 %.

It is noteworthy that the performance of sandwiched structure with LLDPE as the middle layer shows a wide -10 dB bandwidth of 3.7 GHz as compared to AS_5B and AS_7B. This could be possibly because of low complex permittivity value of LLDPE (Table 4.4), which is relatively close to air. As the incident EM wave after passing through layer A, approaches the LLDPE layer, the wave experiences a moderately high impedance mismatch and hence most of the incident power gets reflected. The reflected wave emerging from the A-S interface nearly satisfies λ/4 condition for destructive interference, thereby resulting in a higher bandwidth. In the other structures, i.e., AS_5B and AS_7B, it is seen that when the percentage of EG is increased from zero, the permittivity of the layer increases, thereby allowing the wave to enter the middle layer where it gets further attenuated. With 8 wt. % of EG-LLDPE composite, three resonant peaks of ~-15 dB is observed. Reflection loss of -15.5 dB at 8.45 GHz, -32.3 dB at 10.0 GHz and -16 dB at 11.6 GHz with -10 dB absorption bandwidth of 4.03 GHz covering almost the entire X-band is obtained. The -20 dB bandwidth for the same structure is 0.67 GHz. When the performance of sandwiched structures is compared with the double layer structures, it is seen that reducing the thickness of the ferrite layers and by loading the gap with dielectric layers improves the absorption performance. The performance comparison of the absorber structures is given in table 4.7.

Table 4.7: Experimental (BW_m) and theoretical (BW_c) absorption bandwidth of the fabricated sandwich structures

Absorber structures	Bandwidth (GHz)			
	-10 dB BW_c	-20 dB BW_c	-10 dB BW_m	-20 dB BW_m
ASB	4.2	3.60	3.70	0.34
AS_5B	4.2	3.53	2.60	--
AS_7B	4.2	3.61	3.53	--
AS_8B	4.2	3.63	4.03	0.67

4.4 Conclusion

A double layered absorber is studied and fabricated. An improvement in reflection loss by 4.91% and the absorption bandwidth by 3.5% as compared to the single layer absorber is achieved. Three layered sandwiched absorbing

structures are designed and fabricated by sandwiching a dielectric layer in between two magnetic layers. Appropriate permittivity values of the Layer 2 (S) aids in enhanced of attenuation of the incident wave, thus improving absorption performance of the absorber. The absorber structure is also compact as air which is generally used is replaced by a dielectric layer. A -10 dB bandwidth in excess of 2 GHz is observed in all the structures. When the permittivity of the Layer 2 (S) matches with the other two layers, the wave attenuation increases as does the -10 dB absorption bandwidth, which covers almost the entire X-band.

References:

[1] Gogoi, J. P., Bhattacharyya, N. S. and Bhattacharyya, S. (2014). Single layer microwave absorber based on expanded graphite-novolac phenolic resin composite for X-band applications. *Composites Part B Engineering*, 58: 518–523.

[2] Asi, M. J. and Dib, N. I. (2010). Design of multilayer microwave broadband absorbers using central force optimization. *Progress in Electromagnetic Reserach B*, 26: 101–113.

[3] Reinert, J., Psilopoulos, J., Grubert, J. and Jacob, A. F. (2001). On the potential of graded-chiral dallenbach absorbers. *Microwave and Optical Technology Letters*, 30: 254–257.

[4] Kim J. W. and Kim S. S. (2010). Microwave absorbers of two-layer composites laminate for wide oblique incidence angles. *Materials and Design*, 31:1547–1552.

[5] Zhang, Z., Wang, Z. and Wang, L. (2009). Design principle of single- or double-layer wave-absorbers containing left-handed materials. *Materials and Design*, 30: 3908–3912.

[6] Wei, C., Shena, X., Song, F., Zhu, Y. and Wang, Y. (2012). Double-layer microwave absorber based on nanocrystalline $Zn_{0.5}Ni_{0.5}Fe_2O_4$/α-Fe Microfibers. *Materials and Design*, 35: 363–368.

[7] Feng, Y. B., Qiu, T. and Shen, C.Y. (2007). Absorbing properties and structural design of microwave absorbers based on carbonyl iron and barium ferrite. *Journal of Magnetism and Magnetic Materials*, 318: 8–13.

[8] Liao, Z. Q., Nie, Y., Ren, W., Wang, X. and Gong, R. (2010). Effect of FeCoB–SiO2-film-based fractal frequency selective surface on the absorption properties of microwave absorbers. *IEEE Magnetic Letters*, 1: 5000204.

[9] Chen, M., Zhua, Y., Pana, Y., Koua, H., Xuab, H. and Guoa, J. (2011). Gradient multilayer structural design of CNTs/SiO2 composites for improving microwave absorbing properties, *Materials and Design*, 32: 3013–3016.

[10] Salisbury, W. W. (1952). Absorbent body for electromagnetic waves. US Patent No. 2599944.

[11] Severin, H. (1956). Nonreflecting absorbers for microwave radiation. *IRE Transactions on Antennas and Propagation*, 4: 385–392.

[12] Fante, R. L. and McCormack, M. (1988). Reflection properties of the Salisbury screen. *IEEE Transactions on Antennas and Propagation*, 36: 1443–1454.

[13] Sjoberg, D. (2008). Analysis of wave propagation in stratified structures using circuit analogues, with application to electromagnetic absorbers. *European Journal of Physics*, 29: 721–734.

[14] Meshrama, M. R., Agrawala, N. K., Sinhaa, B. and Misra, P.S. (2004). Characterization of M-type barium hexagonal ferrite-based wide band microwave absorber. *Journal of Magnetism and Magnetic Materials*, 271: 207–214.

[15] Ren, X., Fan, H. and Cheng, Y. (2016). Microwave absorption properties of double-layer absorber based on carbonyl iron/barium hexaferrite composites. *Applied Physics A*, 122, 506–512.

[16] Afgahi, S. S. S., Jafarian, M., Atassi, Y. and C. A. Stergioud. (2017). Single and double-layer composite microwave absorbers with hexaferrite $BaZn_{0.6}Zr_{0.3}X_{0.3}Fe_{10.8}O_{19}$ (X = Ti, Ce, Sn) powders. *Journal of Materials Chemistry and Physics*, 186: 584–591.

[17] Osaka, T. K., Arida, H. T. and Nagoya, K. N. (1998). Multilayer wave absorber. US patent No. 5708435A.

[18] Wright, R. W. and Alexandria, V. (1977). Combined layers in a microwave radiation absorber. US patent No. 4012738A.

[19] Jiang, L., Cui, J., Shi, L. and Li, X. (2009). Pareto optimal design of multilayer microwave absorbers for wide-angle incidence using genetic algorithms. *IET Microwaves, Antennas and Propagation*, 3: 572–579.

[20] Qin, F. and Brosseau, C. (2012). A review and analysis of microwave absorption in polymer composites filled with carbonaceous particles, *Journal of Applied Physics*, 111: 061301-1-24.